Preprints of the 20th World Congress
The International Federation of Automatic Control
Toulouse, France, July 9-14, 2017

Parameter varying flutter suppression control for the BAH jet transport wing ⋆

B. Patartics * **T. Luspay** * **T. Péni** * **B. Takarics** * **B. Vanek** *
T. Kier **

* *Institute for Computer Science and Control (SZTAKI), H-1111 Budapest, Kende u. 13-17.*
** *German Aerospace Center (DLR), Institute of System Dynamics and Control, Munchner Strasse 20, 82234 Oberpfaffenhofen-Wessling*

Abstract: The aeroelastic flutter is an undamped oscillation that occurs on flexible structures placed into an airflow. It is caused by the interaction of the structural dynamics and the aerodynamics. Since it generally leads to structural failure, it has to be avoided. The paper proposes a complete framework for handling the aeroservoelastic behavior of aerospace applications, addressing the high dimensional problem in a tractable manner. The applicability of the proposed methodology is demonstrated by designing a flutter suppression controller for the BAH jet transport wing.

Keywords: aerospace, linear parameter-varying systems, model reduction, robust control

1. INTRODUCTION

The aeroelastic flutter is an undamped oscillation of a flexible structure placed into an airflow. With increasing airflow speed, the structural damping becomes insufficient to compensate the intensifying vibration caused by the aerodynamic forces. The flutter generally leads to poor handling quality and structural destruction, therefore has to be avoided. Conventional aircraft are designed in a way that flutter does not occur under normal operating conditions. This is usually achieved through the use of stiffening materials and thus at the expense of additional structural mass. However, the future trends in aircraft design are oriented to build more economical vehicles, i.e. to increase fuel efficiency and decrease the operating costs. To achieve these goals, increasing the aspect ratio, decreasing the structural mass, and using more flexible components are possible ways to go. On the other hand, in more flexible aircraft the flutter effect can occur during normal operation, hence an active flutter suppression control has to be developed to enlarge the flutter-free operating domain. To cope with this challenging task, several research projects have been launched in the last few years in both EU and US, e.g. (FLEXOP, 2015-2018) and (PAAW, 2014-2019).

In this paper, a complete synthesis framework comprising the control oriented modelling and the model based control design is presented. The procedure is demonstrated by designing a flutter suppression controller for the BAH jet transport wing. This wing was first considered in (Bisplinghoff et al., 1955) and adapted as a flutter demonstration problem in (Rodden et al., 1979).

⋆ The research leading to these results is part of the FLEXOP project. This project has received funding from the Horizon 2020 research and innovation programme of the European Union under grant agreement No 636307.

To design the flutter suppression controller, a suitable dynamical model is needed that captures the flutter phenomenon. One possible method for generating an aeroservoelastic model is based on separately developing a linear structural model and a parameter-varying aerodynamic model and interconnecting them via the modal coordinates and the aerodynamic forces. The structural model can be generated by Finite Element (FE) approach, while the aerodynamic model can be obtained by using a suitable aerodynamic model, for example the Double Lattice Method (DLM) (Albano and Rodden, 1969). This modelling framework forms the base of the commercially available Nastran Aeroleasticity software package (Rodden and Johnson, 1994), where the BAH wing is available as a benchmark example. From a control engineering viewpoint, the resulting models can be generally recast in a Linear Parameter Varying (LPV) form.

In order to capture the flutter effect, an accurate aerodynamic model is needed, which uses a suitably dense structural grid and a large number of lag states. Consequently, the resulting models are high-dimensional, preventing control synthesis due to numerical complexity. Therefore, a model reduction step is needed to decrease the number of states to a manageable size, without effecting the input-output behavior of the system. In this paper, the model reduction methodology presented in (Luspay et al., 2016) is applied to reduce the large dimensional model of the BAH wing. This algorithm has been developed recently and is based on an approximate modal decomposition and parameter-varying balanced truncation (Wood, 1995).

The reduced-order LPV model is used for designing controllers. The controller has to enlarge the flutter-free operating domain (which is considered to be outside of the normal operation domain), while it must not influence the other flight control components on the aircraft. To solve

this multi objective synthesis problem, different control design approaches have been investigated in the literature. Early results follow the *collocated feedback* design methodology, i.e. the sensors and actuators are placed on the same location in order to simplify the underlying control problem. A very similar concept called *identically located force and acceleration* was successfully applied to stabilize the structural modes of the B-1 and B-52 aircraft (Wykes et al., 1980). Despite its early success, several limitations of the collocated control has been explored. First, it is very sensitive to time delays, and second, it cannot be applied if the aeroelastic modes are very close to the rigid-body dynamics (Theis et al., 2016). Due to these limitations, the collocated control has been proven inappropriate for Body Freedom Flutter (BFF) aircraft such as Lockheed Martin's BFF (Holm-Hansen et al., 2010) or the mini MUTT of the UoM (Theis et al., 2016). Therefore a *blend of multivariable quadratic Gaussian (LQG) controllers* are designed for the BFF and *linear time-invariant $\mathcal{H}_\infty$ controller* has been proposed for the mini MUTT (Theis et al., 2016). This paper follows the concept of (Theis et al., 2016), i.e. the flutter suppression problem, which is a stabilization task, is completed with suitable $\mathcal{L}_2$-norm performance criteria and a parameter varying controller is designed by using the LPVTools toolbox of MATLAB (Balas et al., 2015).

The paper is organized as follows. After the introduction, Section 2 outlines the aeroservoelastic modelling of the BAH wing. For the reduction of the resulting high dimensional system, an LPV model reduction algorithm is outlined in Section 3. Section 4 is devoted to the control synthesis and numeric simulation of the closed loop. Finally, the main results are highlighted and the most important conclusions are drawn.

2. AEROSERVOELASTIC MODELLING

The aim of the current section is to present the basic concept and steps of aeroservoelastic modelling of the BAH wing. The BAH wing is a half wing with $b = 12.7\,\mathrm{m}$ half wingspan, $\bar{c} = 4.1275\,\mathrm{m}$ reference chord, and $S = 52.42\,\mathrm{m}^2$ wing area per side. It is fixed at the root and placed in an airflow of varying speed. The model is developed to describe the dynamic behavior of the wing around the flutter onset speed, which is $V_f = 343.11\,\mathrm{m/s}$. The aeroservoelastic model is developed based on a subsystem approach (Kier and Looye, 2009). The aerodynamics and the structural dynamics are developed separately and the interconnection forms the aeroservoelastic model as illustrated in Fig. 1.

The structural model is obtained from a FE approach (Rodden, 1967). A common component of such applications is the Euler-Bernoulli beam with added torsional effects. The mass distribution of the wing is assumed to be replaced by a concentrated mass system based on physical considerations. The ten structural grid points are placed forward and aft along the concentrated masses as seen in Fig. 2 (Rodden and Johnson, 1994; Bisplinghoff et al., 1955). The ten structural grid points have one degree of freedom, heaving in the z direction. Grid point eleven in Fig. 2 is fixed, while grid point twelve represents the control surface deflection and can rotate along the y axis. The structural model can be written as

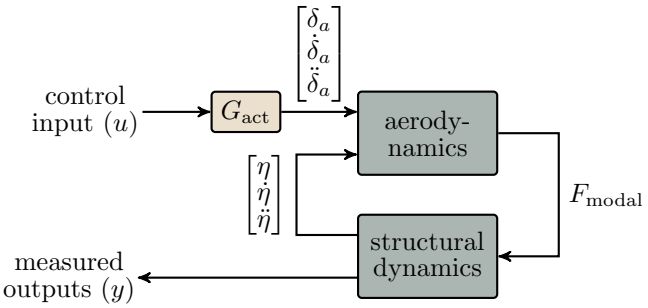

Fig. 1. Aeroelastic model. The δ_a is the control surface deflection, and η is the vector of modal deformations.

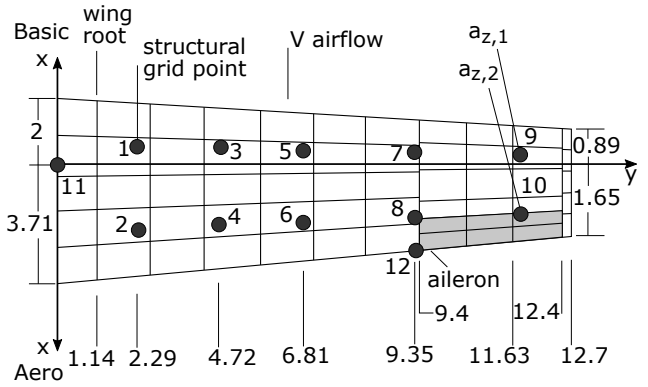

Fig. 2. BAH wing planform and aerodynamic strip idealization.

$$M\ddot{\eta} + C\dot{\eta} + K\eta = F_{\mathrm{ext}_{\mathrm{modal}}}, \tag{1}$$

where M, C, and K are the modal mass, damping, and stiffness matrices respectively, η is the vector of modal deformations, and $F_{\mathrm{ext}_{\mathrm{modal}}}$ is the external excitation in modal coordinates. For the BAH wing model $F_{\mathrm{ext}_{\mathrm{modal}}} = F_{\mathrm{panel}_{\mathrm{modal}}} + F_{\mathrm{cs}_{\mathrm{modal}}}$, where $F_{\mathrm{panel}_{\mathrm{modal}}}$ and $F_{\mathrm{cs}_{\mathrm{modal}}}$ are the external forces in modal coordinates resulting form the aerodynamic panel deformation and control surface deflection respectively. The elastic deformation of the i^{th} structural grid point can be written in terms of the modal coordinates and mode shapes Φ as $\delta_i = \sum_j^n \Phi_{ij}\eta_j$. In the present case, the mode shapes relate the modal coordinates to the structural grid points' heaving motion in z direction. The mode shapes, mass, and stiffness matrices along with the rest of the parameter values of the BAH wing can be found in (Rodden and Johnson, 1994). Note that the damping matrix of the BAH wing's structural model is zero.

The unsteady aerodynamics is modeled with the subsonic DLM (Albano and Rodden, 1969). The model is divided into aerodynamic panels as shown in Fig. 2.

A short summary of the generalized aerodynamic model for the aerodynamic panels is given based on (Rodden and Johnson, 1994; Kotikalpudi et al., 2015). The DLM results in the *AIC* (Aerodynamic Influence Coefficient) matrices, that relate the normalwash vector $\bar{w}$ to the normalized pressure difference vector $\bar{p}$ about the panels as

$$\bar{p}_{\mathrm{panel}} = [AIC_{\mathrm{panel}}(\omega, V)]\,\bar{w}, \tag{2}$$

where ω is the oscillating frequency, and V is the air speed. The ω and V are transformed into a single dimensionless

parameter, the reduced frequency $k = \frac{\omega \bar{c}}{2V}$. In order to relate the modal displacements to the normalwash vector $\bar{w}$, and to transform the aerodynamic force to modal coordinates, the so called generalized aerodynamic matrix (GAM) is introduced (see (Rodden and Johnson, 1994; Kotikalpudi et al., 2015) for more details). This is $Q_{\text{panel}}(k) = \Phi^T T_{\text{as}}^T L \left[AIC_{\text{panel}}(k)\right] (D_1 + ikD_2) T_{\text{as}} \Phi$, where D_1 and D_2 are the differentiation matrices, L is the integration matrix, and T_{as} is the interpolation matrix that projects the structural grid deformation on to the aerodynamic panels in form of their pitch and heave deformation (Kier and Looye, 2009). The GAM maps η to the aerodynamic force distribution in modal coordinates as $F_{\text{panel}_{\text{modal}}} = \bar{q} \left[Q_{\text{panel}}(k)\right] \eta$, where $\bar{q}$ is the free stream dynamic pressure. Since the GAM matrices are frequency dependent, the resulting aerodynamic model is dynamic. Note, that the GAM matrices are obtained only over a discrete reduced frequency grid. However, time domain aeroelastic simulations require a continuous model. There are several methods to obtain such models (Roger, 1977). Roger's rational function approximation (RFA) method (Roger, 1977) was applied for the BAH wing. The resulting aerodynamic model is obtained in the form

$$Q_{\text{panel}}(k) = Q_{\text{panel}_0} + Q_{\text{panel}_1} ik + Q_{\text{panel}_2} (ik)^2 + \sum_{l=1}^{n_p} Q_{\text{panel}_{l+2}} \frac{ik}{ik + b_l}, \tag{3}$$

where Q_{panel_0}, Q_{panel_1}, and Q_{panel_2} stand for the quasi-steady velocity and acceleration terms of the aerodynamic model. The $Q_{\text{panel}_{l+2}}$ terms take the lag behavior of the aerodynamic model into account. The poles of the lag states are given by b_l. For each modal coordinate, the number of poles n_p is selected a priori. This implies that the resulting aerodynamic model in general is of much higher dimension than the structural model. Note, that RFA form of the GAM matrix given as (3) requires the modal coordinates η, and their first and second derivatives as input parameters. In addition, such form of the GAM matrix results in a linear parameter-varying (LPV) aerodynamic model that is affine with respect to the dynamic pressure (V^2).

In a similar fashion, the GAM matrices for the control surface deflection δ_a is defined as

$$F_{\text{cs}_{\text{modal}}} = \bar{q} \left[Q_{\text{cs}}(k)\right] \delta_a, \tag{4}$$

where $Q_{\text{cs}}(k)$ is the control surface GAM matrix. The actuator moving the aileron is modeled by a seventh order linear system taken from (Brenner, 1996):

$$G_{\text{act}}(s) = \frac{2 \cdot 10^{16} (s + 356)}{(s^2 + 2 \cdot 0.62 \cdot 69.1 s + 69.1^2)(s^2 + 2 \cdot 0.94 \cdot 392 s + 392^2)} \cdot \frac{1}{(s^2 + 2 \cdot 0.82 \cdot 746 s + 746^2)(s + 17326)}.$$

The RFA approximation of the control surface GAM matrix $Q_{\text{cs}}(k)$ requires δ_a and its first and second derivatives. These signals are pulled out from the actuator dynamics, so the final model has only one input u, which is the input of the actuator model, as depicted in Fig. 1.

Four signals are defined as the output of the BAH wing model. Two accelerometers are placed on the forward and aft structural grid points at the tip of the wing. Two angular rate sensors are placed at the same cross-section of the wing measuring the local pitch and roll rates respectively. Therefore, $y = [a_{z,1} \; a_{z,2} \; q \; p]^T$.

The structural dynamics of the BAH wing contain the first ten structural modes and their time derivatives. This gives a twenty-state model in the form of (1). The aerodynamic model is constructed by selecting $n_p = 8$ poles for each structural coordinate. Therefore, the aerodynamic model consists of eighty lag states with an additional eight lag states for the aileron input. The aeroelastic model of the BAH wing including the actuator dynamics has therefore 115 states. The structural and actuator models are linear, while the aerodynamic model varies with V^2. The resulting model is thus linear parameter-varying:

$$\begin{aligned} \dot{x}(t) &= A(\rho(t))x(t) + B(\rho(t))u(t) \\ y(t) &= C(\rho(t))x(t) + D(\rho(t))u(t), \end{aligned} \tag{5}$$

where $x(t) \in \mathbb{R}^{115}$. The scheduling parameter $\rho(t) = V(t)$ is defined in the interval [121.92, 640.08] m/s. The time derivative of $\rho(t)$ is assumed to take values from $\Omega = [-5, \; 5]$ m/s^2. The LPV model is given by a set of LTI systems defined by evaluating (5) at 205 equidistant grid points from the interval above. At V_f, the first bending and first torsion modes become coupled.

3. MODEL REDUCTION

The control design for Linear Parameter Varying systems are generally formulated as an optimization problem subject to Linear Matrix Inequality (LMI) constraints over the scheduling parameter domain. It is well-known, that the numerical complexity of these problems grows exponentially with the dimension of the underlying system. Therefore, reduced order models are necessary for the synthesis of parameter-varying controllers. This section discusses the recently developed model reduction methodology (Gőzse et al., 2016; Luspay et al., 2016) from the viewpoint of flutter control design.

First, the operation domain of the full-order system is limited. Since our aim is to suppress the flutter, we limit our focus to a tighter velocity domain $\Gamma = [\rho_{\min}, \; \rho_{\max}] := [122, \; 445]$ m/s. Note, that the divergence occurs around 520 m/s.

The developed model reduction algorithm is based on a modal-like description for LPV systems. The modal form for LTI systems is characterized by the block-diagonal structure of the A matrix, where each block corresponds to an eigenvalue. In order to extend this idea for the LPV system (5), a diagonalizable $A(\rho)$ is necessary. Consequently, the eigendecomposition of the matrix sequence is computed, providing eigenvalues and eigenvectors at every gridpoint. Although local modal forms can be constructed this way, one has to assure the correct ordering of the eigenvalues over the parameter domain. For this purpose, a graph-theoretic solution is offered in (Gőzse et al., 2016; Luspay et al., 2016). The problem is reformulated as a minimum cost perfect-matching problem over bipartite graphs using a suitably chosen distance metric. Numerically effective solutions are known and can be implemented for the underlying problem. Accordingly, consistent ordering of the modal blocks is achieved.

The next step towards the LPV modal form is introduced for ensuring smooth interpolation of the resulting system

over the entire parameter domain. The modal transformation depends on the parameter-varying eigenspace of $A(\rho)$, which can contain arbitrary sign changes, hindering the smooth interpolation. Consequently, it is necessary to correct the eigenvector systems, which is translated into a complex Procrustes-problem. An optimal transformation is sought between neighboring eigenvectors, which renders them as close as possible, but preserves their eigen property. Although, the obtained LPV modal form can be smoothly interpolated between grid points, the parameter-varying transformation introduces $\dot{\rho}$ dependence in the system. At the same time, numerical studies showed that this term can be neglected for BAH wing model.

The obtained LPV modal form is very useful for the analysis and reduction of the system. First of all, unstable parts can be easily identified, separated, and preserved. In the given problem, two state variables, regarding the flutter mode are detached from the dynamics. The remaining 113 states are further reduced by investigating the frequency content of the modes, where thirteen high frequency modes above 80 rad/s are removed.

The remaining hundred states are then grouped into smaller sets, by using hierarchical clustering. The main idea is to brake the system down into smaller subsystems by merging dynamically similar modes together. For this purpose, a similarity measure is defined to compare parameter-varying modes by using the pseudo-hyperbolic metric (Gőzse et al., 2016). At each step of the clustering, those two data objects are merged where the distance metric is the smallest. This is repeated until all modes are merged into a single cluster. For the BAH-wing model, ten dynamical clusters have been created with dimensions 2, 2, 2, 2, 2, 22, 11, 11, 22, and 22. Note that five clusters have only two states, which are related to the structural and actuator dynamics, while the higher dimensional blocks embrace the unsteady aero dynamics. The two-dimensional systems are preserved and only the higher dimensional ones are reduced individually by using standard balancing techniques. For each subsystem, a quadratic controllability, and observability Gramians are computed as $X_c(\rho) = X_{c,0} + \rho X_{c,1} + \rho^2 X_{c,2}$, and $X_o(\rho) = X_{o,0} + \rho X_{o,1} + \rho^2 X_{o,2}$ respectively. The corresponding Lyapunov inequalities are constructed as finite number of LMI constraints by gridding over the admissible parameter domain. The proposed iterative optimization in (Wood, 1995) is solved and the parameter-varying singular values, along with the balancing transformations, were constructed. Consequently the 22, 11, 11, 22, and 22 dimensional subsystems are reduced to 3, 2, 2, 2, and 2, respectively. The parameter-varying transformation introduces an affine $\dot{\rho}$ dependency in the reduced blocks. Unlike in case of the modal transformation, this is not negligible.

Finally, the non-reducible clusters (ten states) and the unstable part (two states) are merged together with the obtained reduced-order (eleven states), stable model. Consequently, a twenty-three-dimensional LPV model is obtained for the approximation of the 115-dimensional BAH-wing dynamics. This model is used as a basis of the flutter control design.

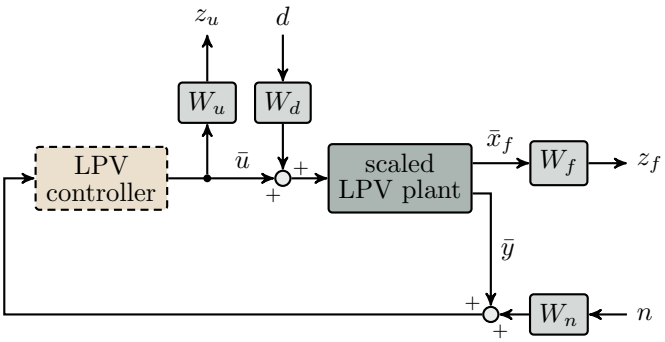

Fig. 3. Generalised plant interconnection for the flutter suppression control design.

4. CONTROL DESIGN

This section is dedicated to describe the LPV controller design technique used to synthesise the flutter suppression controller. The reduced order model can be given in state-space form as

$$\begin{aligned} \dot{x}_r &= A(\rho,\dot{\rho})x_r + B(\rho,\dot{\rho})u \\ y &= C(\rho,\dot{\rho})x_r + D(\rho,\dot{\rho})u, \end{aligned} \tag{6}$$

where $x_r(t) \in \mathbb{R}^{23}$ is the reduced state vector. The control input u and the measured output y are defined in Section 2. The aim of the design is to expand the flight envelope of the aircraft by stabilizing the full order plant (5) over the entire velocity domain Γ. For this, the output vector is completed with two further elements: the two state variables, collected in x_f, that correspond to the flutter mode (i.e. the mode going unstable at V_f) are also selected as outputs. Of course, these two states are not available for measurement, but can be used to formulate performance specifications for the closed loop system.

Scaling. In order to improve the numerical conditioning of the synthesis problem, the reduced order model is scaled such that the inputs and outputs assume values of the same order of magnitude. Expecting that the deflection of the aileron remains between $\pm 20°$, the input is scaled by $S_i = \pi/9$, i.e. u is replaced by $\bar{u} = S_i u$. In order to scale the outputs, the LPV model is evaluated at $\rho = 340.36$ m/s (close to V_f but still in the stable domain) and the step response of the LTI system obtained is analysed. The diagonal scaling matrix S_o is chosen such that the scaled outputs $\left[\begin{smallmatrix}\bar{y}\\ \bar{x}_f\end{smallmatrix}\right] = S_o \left[\begin{smallmatrix}y\\ x_f\end{smallmatrix}\right]$ are all less than 1 in magnitude. Actually, $S_o = 10^{-3} \cdot \mathrm{diag}\,(1.5, 1.3, 3, 2, 319.7, 263.6)$ is used. After scaling, the elements of the $B(\rho,\dot{\rho})$ matrix are of the order of 10^3, while the elements of $C(\rho,\dot{\rho})$ are of the order of 10^{-1}. Thus, a state transformation $\bar{x} = 10^{-2}x$ is applied to balance the matrices. Finally, the scheduling parameter is scaled: ρ is replaced by $\bar{\rho} = \rho/\rho_{\max}$, which implies $\dot{\bar{\rho}} = \dot{\rho}/\rho_{\max}$.

Controller synthesis. Following the concept of (Theis et al., 2016), the flutter suppression problem is formulated as a robust control design task. For this, two performance inputs are introduced: the input disturbance d and the measurement noise n. The generalized plant interconnection can be seen in Fig. 3. The input of the generalised plant is thus $w^T = \begin{bmatrix} n^T & d \end{bmatrix}$, while the output $z^T = \begin{bmatrix} z_f^T & z_u \end{bmatrix}$ is composed of the flutter mode and the actuator effort.

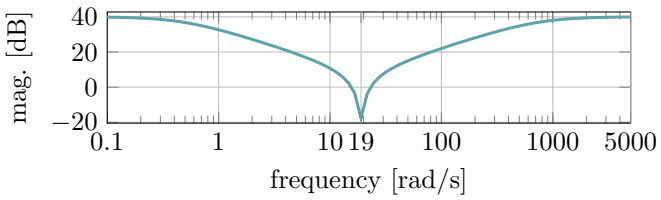

Fig. 4. Bode magnitude plot of the notch filter $W_u(s)$.

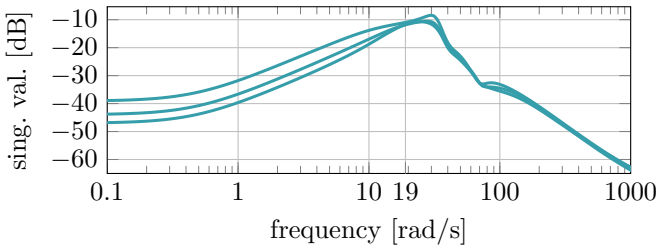

Fig. 5. Singular values of the controller from $\bar{y}$ to $\bar{u}$ at $\rho = 300\,\mathrm{m/s}$, V_f, $400\,\mathrm{m/s}$.

The weighting functions of Fig. 3 are $W_n(s) = 0.001I$, $W_d(s) = 1$, and $W_f(s) = 0.2I$, where I is the identity matrix of the appropriate size. The control effort is weighted with the notch filter $W_u(s) = \frac{100s^2+100s+36100}{s^2+760s+361}$ illustrated in Fig. 4. The idea behind this is to limit actuation to the $\pm 15\%$ frequency interval of the flutter frequency, which is established as 19 rad/s. This way, the use of high frequency control inputs is avoided as well as the flutter suppression controller is separated from the baseline flight control components, which act on low frequency domain if the wing is attached to an aircraft.

For the synthesis of the controller, the method proposed by (Wu, 1995) in Theorem 4.3.2 is applied. This algorithm is implemented in the LPVTools toolbox (Balas et al., 2015) under the name `lpvsyn`. The objective of the design is to minimize the induced $\mathcal{L}_2$-norm from w to z. We want the Lyapunov function of the closed loop to be an affine function of ρ. Therefore, we choose $X(\rho)$ and $Y(\rho)$ in (4.3.5) of (Wu, 1995) to be affine with respect to ρ. This means for example that $X(\rho) = X_0 + X_1\rho$, where X_0 and X_1 are constant matrices.

The parameter grid over which the controller is designed consists of eleven evenly placed points of Γ: $\rho_1 = \rho_{\min}, \ldots, \rho_{11} = \rho_{\max}$ and three points of Ω: $[-5,\ 0,\ 5]\ \mathrm{m/s^2}$ with rate bound $|\dot{\rho}| \leq 5\,\mathrm{m/s^3}$.

The controller obtained from this design has twenty-five states. The singular value plot of the controller for three parameter values close to V_f is shown in Fig. 5. We observe, that the gain of the controller peaks around the flutter frequency, as expected (cf. Fig 4). Thus, the flutter suppression control and actuation of the aircraft's overall motion is separated in frequency.

In Fig. 6, the behavior of the full order system and the full order closed loop is compared. In the singular value plot of the full order system, a resonance peak appears at the flutter frequency near V_f. In the closed loop, let an additive disturbance on $u = S_i^{-1}\bar{u}$ be denoted by d_u.

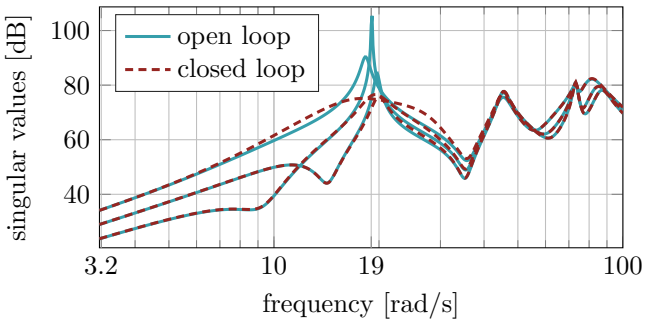

Fig. 6. Singular values of the full order open loop from u to y, and the full order closed loop from d_u to y at $\rho = 300\,\mathrm{m/s}$, V_f, $400\,\mathrm{m/s}$.

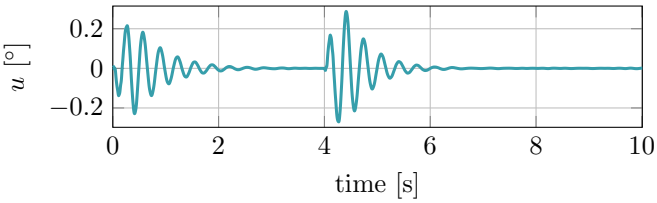

Fig. 7. Value of the controller's output after scaling (i.e. the δ_e command) during the simulation.

Fig. 6 also illustrates the singular value plot of the closed loop from d_u (in radians) to y. Notice, that the resonance peak is suppressed in the closed loop.

Simulation results. A time domain simulation of the closed loop is provided to demonstrate the stability and performance. Due to the limit of space, we only present the first ten seconds of the simulation (but the closed loop remains stable over the entire Γ). During this time, $\rho(t) = 161.5\sin(0.031t + 0.2635) + 284.5$ (in m/s) changes between 325.56 m/s and 371.07 m/s and passes V_f at 3.7 s. The closed loop is excited through d_u, which is 2° until the fourth second and 0° afterwards. This means the aileron is initially deflected to 2° and the disturbance vanishes right after the flutter speed is reached.

The output of the controller after scaling (the actual δ_e command) is depicted in Fig. 7. Evaluating the frequency range of u, we establish, that its dominant frequency component is approximately 19 rad/s, which is consistent with the design specification expressed in $W_u(s)$. Based on Fig. 7, the flutter can be suppressed with small aileron deflections. This is important when the wing is attached to an aircraft, because small deflections induce small torques and forces along the wing leaving sufficient room for actuation to control the overall motion of the aircraft.

The output of the nonlinear BAH wing model is shown in Fig. 8. The change of the disturbance value causes oscillations in the accelerations and angular rates. However, the amplitude of the oscillations decreases, and the controller manages to stabilize the closed loop even beyond the flutter speed. Using this controller, the flight envelope was expanded by 102 m/s.

For physical insight, we present the outputs of the BAH wing in terms of displacements and angles as well. Let the z coordinate of the ninth and tenth structural grid points in Fig. 2 be z_1 and z_2 respectively. The local pitch and roll

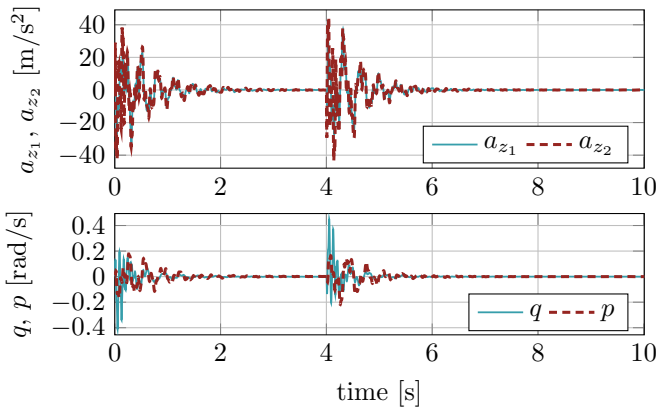

Fig. 8. Value of the BAH wing's output during the simulation.

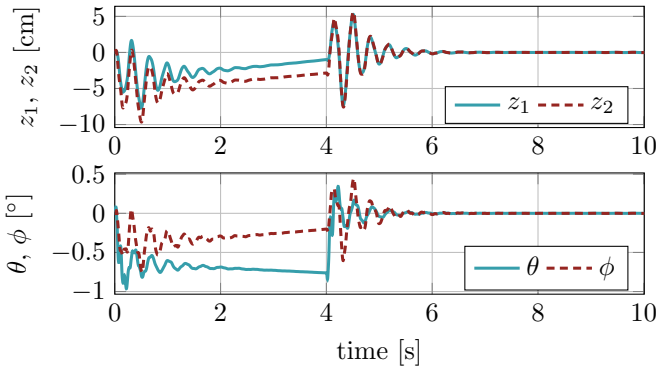

Fig. 9. Value of the displacements and angles related to the BAH wing's output during the simulation.

rates are denoted by θ and ϕ respectively. In other words $a_{z,1} = \ddot{z}_1$, $a_{z,2} = \ddot{z}_2$, $q = \dot{\theta}$, and $p = \dot{\phi}$ assuming zero initial values for all quantities. According to Fig. 9, the maximal heaving of the wing tip is around 10 cm, which is less than 1% of b. The θ and ϕ are less than 1°, which means small deformations of the wing.

5. CONCLUSION

The problem of active flutter suppression is addressed in the paper. A complete control synthesis procedure is proposed: given the large-scale aeroelastic model in LPV form, an efficient model reduction technique is presented, which makes the model numerically tractable for the control synthesis algorithms. The flutter suppression problem is then formulated as a robust control design problem, where the performance requirements are defined via induced $\mathcal{L}_2$ norm conditions. The applicability of the method is demonstrated by designing a flutter suppression controller for the BAH jet transport wing. The methodology will be applied to the full aircraft control problem of the FLEXOP demonstrator and will be flight tested in 2018.

REFERENCES

Albano, E. and Rodden, W. (1969). A doublet-lattice method for calculating lift distributions on oscillating surfaces in subsonic flows. *Journal of Aircraft*, 7(2), 279–285.

Balas, G., Hjartarson, A., Packard, A., and Seiler, P. (2015). *LPVTools: A Toolbox for Modeling, Analysis, and Synthesis of Parameter Varying Control Systems*. Musyn, Inc. URL `http://www.aem.umn.edu/~SeilerControl/software.shtml`.

Bisplinghoff, R.L., Ashley, H., and Halfman, R.L. (1955). *Aeroelasticity*. Addison-Wesley Publishing Company.

Brenner, M.J. (1996). Aeroservoelastic Modeling and Validation of a Thrust-Vectoring F/A-18 Aircraft. Technical report, NASA, Dryden Flight Research Center.

FLEXOP (2015-2018). Flutter Free FLight Envelope eXpansion for ecOnomical Performance improvement (FLEXOP). Project of the European Union, Project ID: 636307.

Gőzse, I., Luspay, T., Péni, T., Szabó, Z., and Vanek, B. (2016). Model Order Reduction of LPV Systems Based on Parameter Varying Modal Decomposition. In *IEEE Conference on Decision and Control*.

Holm-Hansen, B., Atkinson, C., Benarek, J., Burnett, E., Nicolai, L., and Youssef, H. (2010). Envelope Expansion of a Flexible Flying Wing by Active Flutter Suppression. In *Association for Unmanned Vehicle Systems International*.

Kier, T.M. and Looye, G.H.N. (2009). Unifying manoeuvre and gust loads analysis models. In *International Forum on Aeroelasticity and Structural Dynamics (IFASD)*.

Kotikalpudi, A., Pfifer, H., and Balas, G.J. (2015). Unsteady Aerodynamics Modeling for a Flexible Unmanned Air Vehicle. In *AIAA Atmospheric Flight Mechanics Conference*.

Luspay, T., Péni, T., Gőzse, I., Szabó, Z., and Vanek, B. (2016). Model reduction for LPV systems based on approximate modal decomposition. *Submitted to Int. J. of. Robust Nonlin. Control, but can be accessed in arXiv under reference number arXiv:1609.06948*.

PAAW (2014-2019). Performance Adaptive Aeroelastic Wing Program. Supported by NASA NRA "Lightweight Adaptive Aeroelastic Wing for Enhanced Perfromace Across the Flight Envelope".

Rodden, W.P. (1967). A method for deriving structural influence coefficients from ground vibration tests. *AIAA Journal*, 5(5), 991–1000.

Rodden, W.P., Harder, R.L., and Bellinger, E.D. (1979). Aeroelastic Addition to NASTRAN. Technical report, NASA Contractor Report 3094.

Rodden, W.P. and Johnson, E. (1994). MSC/NASTRAN Aeroelastic Analysis: User's Guide, Version 68.

Roger, K.L. (1977). Airplane Math Modeling Methods for Active Control Design. Structural Aspects of Active Controls. In *Structural Aspects of Active Controls, AGARD-CP-228*, 4–11.

Theis, J., Pfifer, H., and Seiler, P. (2016). Robust Control Design for Active Flutter Suppression. In *AIAA Atmospheric Flight Mechanics Conference*.

Wood, G.D. (1995). *Control of Parameter-Dependent Mechanical Systems*. Ph.D. thesis, University of Cambridge.

Wu, F. (1995). *Control of Linear Parameter Varying Systems*. Ph.D. thesis, University of California at Berkeley.

Wykes, J.H., Byar, T.R., MaeMiller, C.J., and Greek, D.C. (1980). Analyses and Tests of the B-1 Aircraft Structural Mode Control System. Technical report, Contractor Report 144887, NASA.